Circuit model of transient cross-coupling

Ian Brook Darney

Bristol, UK
E-mail: iandarney@blueyonder.co.uk

Published in *The Journal of Engineering*; Received on 10th September 2017; Accepted on 17th November 2017

Abstract: Using a signal generator and an oscilloscope, measurements were made of the differential-mode current and the common-mode current in a twin-conductor cable installed on a test rig, over a range of frequencies which included half-wave resonances. Test data was used to assign component values to a Triple-T circuit model of the assembly. This model was then transformed into a transient coupling model. The signal generator was reset to generate square waves, and photographs were taken of the waveforms of the input voltage and the common-mode current. A close correlation was achieved between these waveforms and those of the transient coupling model. This demonstrates that the technique of circuit modelling and bench testing is reliable and accurate, in both the frequency domain and the time domain. The technique allows potential hazards due to transient interference to be analysed, tested, and quantified during the design process. Electromagnetic interference can be analysed without recourse to the mathematics of full-field modelling. It is also shown that, from the point of view of Electromagnetic Compatibility, the concepts of the single-point ground and the equipotential ground are both misleading and counter-productive.

1. Introduction

It is possible to analyse the mechanisms involved in propagating transient electromagnetic interference (EMI) in any signal link in any electrical system installed on a vehicle, be that a car, lorry, tank, ship, aircraft or spacecraft, and to determine its electromagnetic compatibility (EMC) long before the equipment is submitted to an EMC Test House. This can be done using analytical tools familiar to every electrical engineer; the tools of Circuit Theory. Although the mechanisms involved are those defined by Electromagnetic Theory, there is no need to invoke the complex mathematics of full-field modelling.

There is a clear need for engineers to acquire such abilities. With the increasing sensitivity of digital circuitry and the increasing rate of change of current transients in power supplies, it is necessary to identify and analyse all sorts of hazardous conditions. It is likely that the explosion in the central fuel tank of TWA Flight 800 was caused by intra-system interference.

The best way of illustrating the technique is to build a test rig which involves the coupling between the differential-mode loop and the common-mode loop of a representative signal link. The construction of such a rig is described, as is the circuitry of the interface at the near end. The terminals at the far end are short circuited. The test equipment is extremely simple; a signal generator, an oscilloscope, and a current transformer.

A circuit model which simulates coupling in the frequency domain is described, and component values assigned using data on the geometry of the assembly. A test is carried out to record the variation of differential-mode current with frequency. A similar test is used to record the variation of the amplitude of the common-mode current. An essential feature of these tests is that it covers the frequencies of half-wave resonance of both circuit loops.

A comparison was carried out of the responses of the model and that of the test results. Initially, there was a significant deviation. However, this was corrected by using a process of successive approximation of the components of the model. The resulting model provides a good correlation between theoretical and actual responses in the frequency domain.

A general circuit model which simulates coupling in the time domain is described. The component values are derived from those measured by the frequency response tests. The equations are derived which allow the amplitude of reflections at each end to be computed, and a Mathcad program described which simulates the propagation of energy back and forth along the assembly. The mechanism is analysed in terms of the propagation of discrete packets of charge.

The signal generator was then set to generate square-wave pulses and the oscilloscope used to monitor the waveform of the input voltage to the test rig and the waveform of the differential-mode current. A good correlation was achieved between the actual responses of the hardware and the simulation of the model. The same was done for the common-mode loop.

The model was used to simulate the response of the setup to a step input voltage and the steady-state values of the currents computed. These proved to be exactly the same as those derived from DC analysis.

The results of this set of tests demonstrate the modelling technique is highly reliable, indicating that it can be used during the circuit design process of any electrical system mounted on a conducting structure.

The fallacy in the concept of the 'single point ground' is identified, and it is shown that there is no such thing as an equipotential conductor.

The naming of variables and constants follows the normal practice in computer programming and assigns several characters to each parameter. For example, *RL1*, *RL2* and *RL3* represent the values of the three resistors of the load circuitry. As far as possible, subscripts are used to identify the elements of vectors and matrices.

2. Frequency analysis

2.1. Initialisation

Basically, the rig consisted of a copper pipe installed round the walls of a room. A wooden batten was fixed along the length of the pipe and a twin-conductor cable routed along the surface of the batten. This construction allowed a reasonably constant spacing between cable and pipe to be maintained along the length of the assembly. This configuration can be correlated with any signal link on any vehicle, aircraft, spacecraft, or ship. The copper pipe represents the electrical properties of the conducting

This is an open access article published by the IET under the Creative Commons Attribution License (http://creativecommons.org/licenses/by/3.0/)

doi: 10.1049/joe.2017.0382

structure. In this context, the terms 'conducting structure', 'ground' and 'earth' are synonymous. Details are

– radius of send and return conductors: $r11 = r22 = 0.61$ mm
– radius of pipe: $r33 = 7.5$ mm
– separation between conductors: $r12 = 2.45$ mm
– separation of conductors from pipe: $r13 = r23 = 23$ mm
– length of assembly: $len = 11.4$ m.

The reactive parameters were calculated using [1]

$$\begin{aligned} Lc1 &= \frac{\mu_o \cdot \mu_r \cdot \mathrm{l_{en}}}{2 \cdot \pi} \cdot \ln\left(\frac{r12 \cdot r13}{r11 \cdot r23}\right) = 3.17 \times 10^{-6}\ \mathrm{H} \\ Lc2 &= \frac{\mu_o \cdot \mu_r \cdot \mathrm{l_{en}}}{2 \cdot \pi} \cdot \ln\left(\frac{r12 \cdot r23}{r22 \cdot r13}\right) = 3.17 \times 10^{-6}\ \mathrm{H} \\ Lc3 &= \frac{\mu_o \cdot \mu_r \cdot \mathrm{l_{en}}}{2 \cdot \pi} \cdot \ln\left(\frac{r13 \cdot r23}{r33 \cdot r12}\right) = 7.66 \times 10^{-6}\ \mathrm{H} \end{aligned} \tag{1}$$

$$\begin{aligned} Cc1 &= \frac{2 \cdot \pi \cdot \varepsilon_o \cdot \varepsilon_r \cdot l_{\mathrm{en}}}{\ln\left(\frac{r12 \cdot r13}{r11 \cdot r23}\right)} = 4.56 \times 10^{-10}\ \mathrm{F} \\ Cc2 &= \frac{2 \cdot \pi \cdot \varepsilon_o \cdot \varepsilon_r \cdot l_{\mathrm{en}}}{\ln\left(\frac{r12 \cdot r23}{r22 \cdot r13}\right)} = 4.56 \times 10^{-10}\ \mathrm{F} \\ Cc3 &= \frac{2 \cdot \pi \cdot \varepsilon_o \cdot \varepsilon_r \cdot l_{\mathrm{en}}}{\ln\left(\frac{r13 \cdot r23}{r33 \cdot r12}\right)} = 1.89 \times 10^{-10}\ \mathrm{F} \end{aligned} \tag{2}$$

Resistances of the three conductors were assumed to be

$$\begin{aligned} Rc1 &= 0.2\ \Omega \\ Rc2 &= 0.2\ \Omega \\ Rc3 &= 0.01\ \Omega \end{aligned} \tag{3}$$

2.2. Test setup

A schematic diagram of the test setup is shown in Fig. 1*a*. This includes the interface module which links the test rig to the test equipment. The signal generator provides a voltage *Vin* across the 10 Ω resistor via a 41 Ω resistor. The voltage across the 10 Ω resistor is monitored by channel 1 of the oscilloscope. This configuration allows the impedance presented to the generator to be 50 Ω and the source resistance *Rs*1 applied to the cable input terminals to be

$$Rs1 = \frac{1}{\frac{1}{10} + \frac{1}{41+50} + \frac{1}{41+50}} = 8.2\ \Omega \tag{4}$$

This resistance is significantly less than the impedance presented by the cable assembly over the range of frequencies involved in obtaining test data. So the alternating voltage applied to the assembly-under-review is reasonably constant.

A current transformer was clamped round the send conductor to allow the differential-mode current to be monitored. There were ten turns on the secondary winding, to ensure that the impedance presented to the cable was very low; about 0.24 Ω. Details of the construction and calibration of this transformer are provided by Darney [2].

The three terminals at the near end of the test rig were connected to the interface module as illustrated in Fig. 1*a* and the terminals at the far end were shorted together.

2.3. Test procedure

The signal generator was used to apply a sinusoidal signal to the cable at a set of spot frequencies, over the range of 100 kHz to 12 MHz. Measurements were taken of the peak-to-peak voltages *Vch1* and *Vch2* displayed by the oscilloscope. Since *Vch1* is proportional to *Vin* and *Vch2* is proportional to the current *Idiff* in the differential-mode loop, it was possible to calculate the ratio *Yt1* at each spot frequency

$$Yt1 = \frac{Idiff}{Vin} \tag{5}$$

Yt1 is a measure of the current which would flow in the differential-mode loop when the input voltage was 1 V. The blue circles in Fig. 2*a* show the variation of this parameter with the frequency.

The current transformer was then clamped round both cable conductors and the test repeated. The blue circles in Fig. 2*b* are a record of the variation of the parameter *Yt2* with frequency, where

$$Yt2 = \frac{Icm}{Vin} \tag{6}$$

and *Icm* is the common-mode current.

2.4. Creating the model

The differential-mode current is defined here as that which flows along the send conductor and back along the return conductor. The common-mode current is defined as that which flows along the return conductor and back along the ground.

The part of the model which simulates the test rig can be described as a Triple-T network, with each T-network representing the properties of one conductor. In order to provide an accurate simulation of the frequency response of the assembly-under-test, it was necessary to transform the impedance value of each branch of the network into a distributed parameter.

For the send conductor, the transformations are

$$\begin{aligned} Zh1 &= Zo1 \cdot \tanh\left(\frac{\theta_1}{2}\right) \\ Zv1 &= Zo1 \cdot \mathrm{cosech}\left(\theta_1\right) \end{aligned} \tag{7}$$

where

$$\begin{aligned} Zo1 &= \sqrt{\frac{Rc1 + j \cdot \omega \cdot Lc1}{Gc1 + j \cdot \omega \cdot Cc1}} \\ \theta 1 &= \sqrt{\left(Rc1 + j \cdot \omega \cdot Lc1\right) \cdot \left(Gc1 + j \cdot \omega \cdot Cc1\right)} \end{aligned} \tag{8}$$

and

$$\omega = 2 \cdot \pi \cdot f \tag{9}$$

The impedance *Zh1* replaces the impedances of the horizontal branches representing conductor 1, whilst *Zv1* replaces the impedance of the vertical branch. The same transformations apply to the other two conductors [3].

2.5. Computations

A Mathcad worksheet was compiled to convert the impedance of each branch of the network to a distributed parameter at each frequency and then to calculate the values of the currents *Ic1*, *Ic2*, *Ic3*, and *Ic4*. The admittance *Ym1* is the ratio of the differential-mode current *Ic1* to the voltage *Vin*, and the variation of *Ym1* with

This is an open access article published by the IET under the Creative Commons Attribution License (http://creativecommons.org/licenses/by/3.0/)

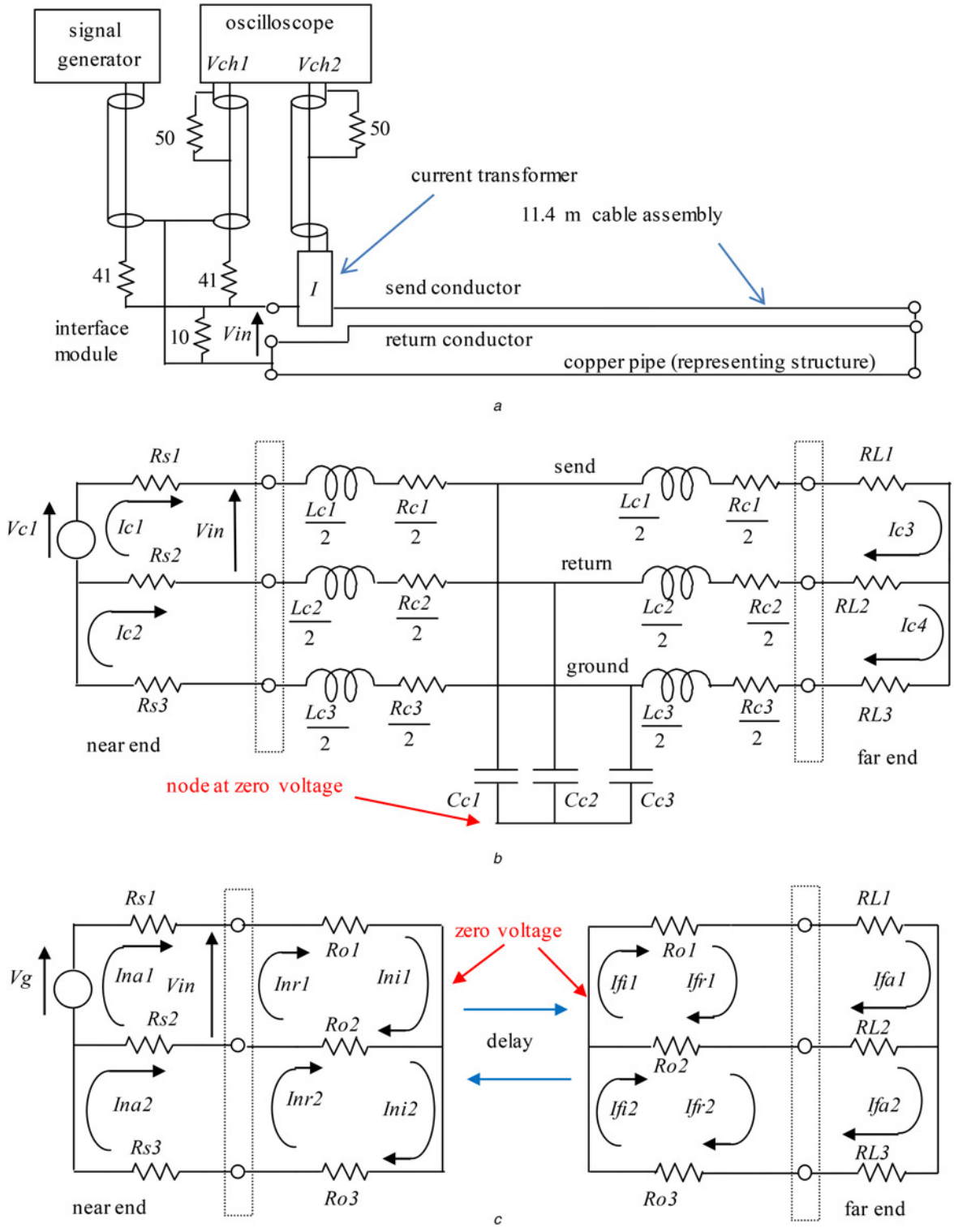

Fig. 1 *Characterising the assembly*
a Test setup
b Lumped-parameter model
c Transient model

frequency is illustrated by the solid red curve in Fig. 2*a*. The transfer admittance *Ym2* in Fig. 2*b* illustrates the variation of the common-mode current *Ic2* with frequency when $Vin = 1$ V.

In the worksheet, the initial values of the lumped parameters were those defined by (1)–(4). When the frequency response of the model was first compared with that of the test results, there was a significant deviation between the solid red curves and the blue circles of Figs. 2*a* and *b*. However, a few iterations of the program, with different values assigned to these lumped parameters, yielded the response illustrated. The process is similar to the iterative method used by computers to solve equations. A full description of the technique is provided by Darney [4]. A copy of the Mathcad worksheet used to perform the computations can be downloaded from [5].

This is an open access article published by the IET under the Creative Commons Attribution License (http://creativecommons.org/licenses/by/3.0/)

doi: 10.1049/joe.2017.0382

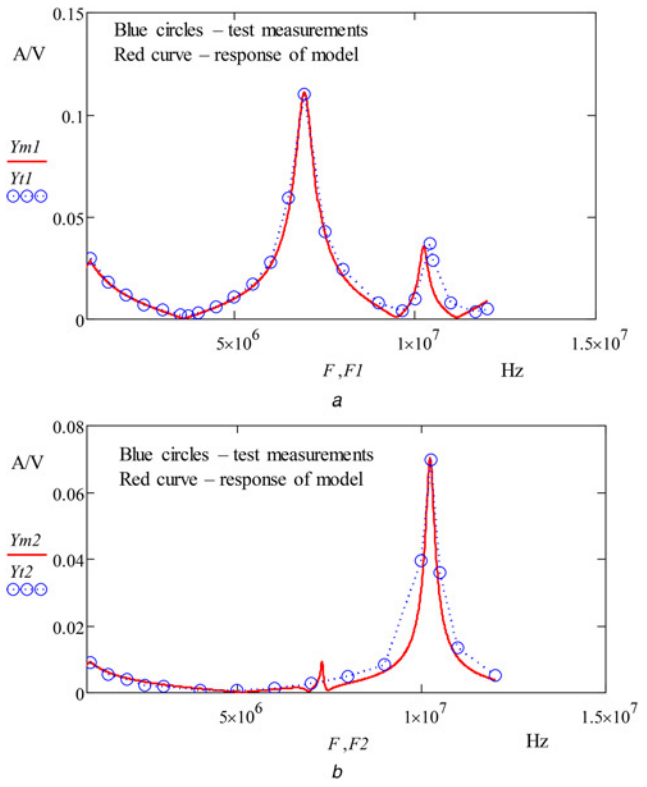

Fig. 2 *Correlation between test results and circuit model*
a Ratio of differential-mode current to input voltage
b Ratio of common-mode current to input voltage

2.6. *Representative circuit model*

The end result was a circuit model which characterises the cross-coupling mechanism of the assembly-under-review. The refined values of the capacitors were

$$\begin{aligned} Cc1 &= 1.73 \times 10^{-9}\ \text{F} \\ Cc2 &= 1.73 \times 10^{-9}\ \text{F} \\ Cc3 &= 3.0 \times 10^{-10}\ \text{F} \end{aligned} \tag{10}$$

These values are significantly higher than those of (2) because of the presence of the insulating material. The average relative permittivities are much greater than unity. The values assigned to the inductors were

$$\begin{aligned} Lc1 &= 3.0 \times 10^{-6}\ \text{H} \\ Lc2 &= 3.0 \times 10^{-6}\ \text{H} \\ Lc3 &= 6.7 \times 10^{-6}\ \text{H} \end{aligned} \tag{11}$$

These are not much different from those of (1). Since this particular set of tests did not provide refined values for the resistors, the values assumed in (3) remain unchanged.

Assigning these new values to the components of Fig. 1*b* results in the representative circuit model of the assembly; one which can be used to define the mechanisms involved in the propagation of electromagnetic interference. It can be modified to predict the EMI of a similar system, whatever the values of the interface components, and whatever the length of the assembly.

The first peak in the response illustrated in Fig. 2*a* is due to resonance of the differential-mode current at its half-wave frequency. This was measured to be

$$fh1 = 6.93 \times 10^6\ \text{Hz} \tag{12}$$

The first peak in the response of the common-mode loop is illustrated in Fig. 2*b*. The half-wave frequency of the common-mode loop was measured to be

$$fh2 = 10.26 \times 10^6\ \text{Hz} \tag{13}$$

The fact that *fh2* is higher than *fh1* means that the common-mode currents and voltages travel faster than the differential-mode signals.

3. Transient analysis

3.1. *Charge propagation*

One of the deductions of Electromagnetic Theory is that when a step voltage is applied to the near end of a lossless transmission line, a step current is induced [6]. Electromagnetic energy propagates along the cable at a speed comparable to that of light in a vacuum and appears at the far end as a constant current which flows into the load. If the velocity of propagation is v, then the time taken to propagate along a line of length *len* is

$$T = \frac{len}{v} \tag{14}$$

If the line is represented as a set of n segments of equal length, then the time for the step to flow along one segment is

$$dt = \frac{T}{n} \tag{15}$$

This definition means that the parameter dt is finite. During time dt, constant current *In* will flow into the near end and the charge delivered to the first segment at a time $t = 0 + dt$ will be

$$Qn = In \cdot dt \tag{16}$$

This charge propagates to the far end and arrives there at the time $t = T$. During the time dt, the current *If* delivered to the far end is

$$If = \frac{Qf}{dt} \tag{17}$$

That is, the line can be represented as a set of segments which carry discrete packages of charge flowing at a near-light velocity. This reasoning can also be applied to the three-conductor line of Fig. 1*c*.

The ratio of the amplitude of the voltage step to that of the current step is a constant and can be defined as the characteristic resistance [7]. The characteristic resistances of the three conductors are

$$\begin{aligned} Ro1 &= \sqrt{\frac{Lc1}{Cc1}} \\ Ro2 &= \sqrt{\frac{Lc2}{Cc2}} \\ Ro3 &= \sqrt{\frac{Lc3}{Cc3}} \end{aligned} \tag{18}$$

3.2. *Partial parameters*

Transmission line theory introduces the concept of partial currents and partial voltages to simulate the behaviour of a twin-conductor line. For a three-conductor line, the number of interdependent variables increases significantly. *Vna1* and *Ina1* identify the voltage and current absorbed at the near end of the differential-mode loop, *Vni1*

This is an open access article published by the IET under the Creative Commons Attribution License (http://creativecommons.org/licenses/by/3.0/)

and *Ini1* identify the incident voltage and current at that end, while *Vnr1* and *Inr1* identify the reflected currents. At the far end, the letter *n* is replaced by the letter *f*. For the common-mode loop, the character *1* is replaced by the character *2*.

3.3. Reflection equations

The set of equations defining their relationship is

$$\begin{aligned} Vni1 + Vnr1 + Vg &= Vna1 \\ Vni2 + Vnr2 &= Vna2 \end{aligned} \tag{19}$$

$$\begin{aligned} Ini1 + Inr1 &= Ina1 \\ Ini2 + Inr2 &= Ina2 \end{aligned} \tag{20}$$

$$\begin{aligned} Vni1 &= (Ro1 + Ro2) \cdot Ini1 - Ro2 \cdot Ini2 \\ Vni2 &= -Ro2 \cdot Ini1 + (Ro2 + Ro3) \cdot Ini2 \end{aligned} \tag{21}$$

$$\begin{aligned} Vnr1 &= -(Ro1 + Ro2) \cdot Inr1 + Ro2 \cdot Inr2 \\ Vnr2 &= Ro2 \cdot Inr1 - (Ro2 + Ro3) \cdot Inr2 \end{aligned} \tag{22}$$

$$\begin{aligned} Vna1 &= (Rs1 + Rs2) \cdot Ina1 - Rs2 \cdot Ina2 \\ Vna2 &= -Rs2 \cdot Ina1 + (Rs2 + Ro3) \cdot Ina2 \end{aligned} \tag{23}$$

In vector–matrix form, these equations are

$$\boldsymbol{Vni} + \boldsymbol{Vnr} + \boldsymbol{Vgen} = \boldsymbol{Vna} \tag{24}$$

$$\boldsymbol{Ini} + \boldsymbol{Inr} = \boldsymbol{Ina} \tag{25}$$

$$\boldsymbol{Vni} = \boldsymbol{Ro} \times \boldsymbol{Ini} \tag{26}$$

$$\boldsymbol{Vnr} = -(\boldsymbol{Ro} \times \boldsymbol{Inr}) \tag{27}$$

$$\boldsymbol{Vna} = \boldsymbol{Rs} \times \boldsymbol{Ina} \tag{28}$$

Subtracting (27) from (26)

$$\boldsymbol{Vni} - \boldsymbol{Vnr} = \boldsymbol{Ro} \times (\boldsymbol{Ini} + \boldsymbol{Inr}) \tag{29}$$

Invoking (25)

$$\boldsymbol{Vni} - \boldsymbol{Vnr} = \boldsymbol{Ro} \times \boldsymbol{Ina} \tag{30}$$

Using (28) to substitute for $\boldsymbol{Vna}$ in (24)

$$\boldsymbol{Vni} + \boldsymbol{Vnr} + \boldsymbol{Vgen} = \boldsymbol{Rs} \times \boldsymbol{Ina} \tag{31}$$

Adding (30) and (31)

$$2 \cdot \boldsymbol{Vni} + \boldsymbol{Vgen} = (\boldsymbol{Ro} + \boldsymbol{Rs}) \times \boldsymbol{Ina} \tag{32}$$

this gives

$$\boldsymbol{Ina} = (\boldsymbol{Ro} + \boldsymbol{Rs})^{-1} \times (2 \cdot \boldsymbol{Vni} + \boldsymbol{Vgen}) \tag{33}$$

3.4. Propagation mechanism

Given knowledge of $\boldsymbol{Ini}$, $\boldsymbol{Vni}$ can be calculated using (26). Then $\boldsymbol{Ina}$ can be calculated using (33). The partial currents $\boldsymbol{Inr}$ delivered to the cable can be derived from (25) and the charges delivered to the differential-mode loop and the common-mode loop during time *dt* will be

$$\boldsymbol{Qnr} = \boldsymbol{Inr} \cdot dt \tag{34}$$

After a short interval, these charges will arrive at the far end and the partial currents delivered at this end during time d*t* will be

$$\boldsymbol{Ifi} = \boldsymbol{Qfi} \cdot \frac{1}{dt} \tag{35}$$

If there are radiation losses, then the charges $\boldsymbol{Qfi}$ arriving at the far end will be less than $\boldsymbol{Qnr}$. The incident voltages will be

$$\boldsymbol{Vfi} = \boldsymbol{Ro} \times \boldsymbol{Ifi} \tag{36}$$

By analogy with (33), the currents $\boldsymbol{Ifa}$ absorbed at the far end will be

$$\boldsymbol{Ifa} = (\boldsymbol{Ro} + \boldsymbol{RL})^{-1} \times (2 \cdot \boldsymbol{Vfi}) \tag{37}$$

The currents reflected at the far end will be

$$\boldsymbol{Ifr} = \boldsymbol{Ifa} - \boldsymbol{Ifi} \tag{38}$$

and the charges sent back down the line during time *dt* will be

$$\boldsymbol{Qfr} = \boldsymbol{Ifr} \cdot dt \tag{39}$$

The time taken for a charge package to propagate from one end of the differential-mode loop to the other is

$$T1 = \frac{1}{2 \cdot fh1} = 7.22 \times 10^{-8}\ \text{s} \tag{40}$$

The time taken for charges in the common-mode loop to travel the same distance is

$$T2 = \frac{1}{2 \cdot fh2} = 4.87 \times 10^{-8}\ \text{s} \tag{41}$$

where *fh1* and *fh2* are defined by (12) and (13).

3.5. Computations

If it is assumed that the differential-mode loop is divided into $n1 = 15$ segments, then the time increment *dt* will be

$$dt = \frac{T1}{n1} = 4.81 \times 10^{-9}\ \text{s} \tag{42}$$

Charges in the common-mode loop travel much faster. So the number of segments which represents this loop will be

$$n2 = \text{ceil}\left(n1 \cdot \frac{T2}{T1}\right) = 11 \tag{43}$$

In Mathcad, the function ceil(x) returns the least integer which is greater or equal to x.

It has been observed that when a step pulse was delivered to the near end of a twin-conductor line which was open-circuit at the far end, the current arriving at that end increased exponentially. A simple R-C circuit was used to simulate the current lost. The current arriving at the far end was reasoned to be the current delivered to the near end, minus the current lost due to radiation [8]. The virtual component which carried the radiated current was assigned the name *Crad*. On that occasion, the value of this parameter was measured to be 250 pF.

Thermal losses due to currents in the series resistances of the conductors can be simulated by assuming they are the properties of the source. That is

$$\begin{aligned} Rs1 &= 8.2 + Rc1 = 8.4 \\ Rs2 &= 0 + Rc2 = 0.2 \\ Rs3 &= 0 + Rc3 = 0.01 \end{aligned} \tag{44}$$

The current transformer of Fig. 1*a* makes its own contribution to the overall response of the system. So its effect needs to be included in any simulation. The model for frequency analysis is illustrated

This is an open access article published by the IET under the Creative Commons Attribution License (http://creativecommons.org/licenses/by/3.0/)

doi: 10.1049/joe.2017.0382

by Figure 7.2.7 of [2]. For transient analysis, it can be represented by a current source *Isec* in parallel with a resistance *RT* and an inductance *LT*.

The mesh equations for this model are

$$\begin{aligned} Vmon &= RT \cdot Isec - RT \cdot Iind \\ 0 &= -RT \cdot Isec + RT \cdot Ind + LT \cdot \frac{dIind}{dt} \end{aligned} \tag{45}$$

where *Vmon* is the voltage across *RT*, *Iind* is the current in the inductance and *dIind*/*dt* is the rate of change of current in *LT*. From this, it can be deduced that the sequence of computations is

$$dIind \leftarrow \frac{dt}{LT} \cdot RT \cdot (Isec - Iind) \tag{46}$$

$$Iind \leftarrow Iind + dIind \tag{47}$$

$$Vmon \leftarrow RT \cdot (Isec - Iind) \tag{48}$$

where *Iind* in (46) is the value stored in the previous computation and

$$Isec = \frac{Iprim}{Turns} \tag{49}$$

This set of computations gives the value of the transient voltage *Vmon* appearing at channel 2 of the oscilloscope, given knowledge of the current *Iprim* in the primary of the transformer and the previous value of *Iind*.

3.6. Mathcad worksheet

Figs. 3–5 are copies of pages 1, 2 and 3 of the Mathcad worksheet which has been devised to simulate the transient performance of the setup of Fig. 1*a*. Essentially, the worksheet has been derived from the circuit model of Fig. 1*c*.

The first page of the worksheet is a definition of the input variables and input constants used in the computations. The first two lines define the values for the inductors and capacitors. They are the values derived from the frequency analysis; (10) and (11). The values of *Rs1*, *Rs2,* and *Rs3* are those defined by an equation set (44). The values for *RL1*, *RL2*, and *RL3* are zero because the terminations at the far end are short circuited. The values for *Crad1* and *Crad2* were set after a few iterations of the transient analysis. There are ten turns on the secondary winding of the current transformer. Hence, *Turns* = 10.

The values for the resistance *RT* and the inductance *LT* of the current transformer are the same as the values defined in [2]. The value of *K* is the ratio of *Vin* to the voltage monitored at channel 1 of the oscilloscope, *Vch1*, as shown in Fig. 1*a*. The equations for *Ro1*, *Ro2* and *Ro3* are defined by (18).

Vg is the value of the source voltage necessary to develop a step input voltage of 0.8 V at channel 1 of the oscilloscope during the first transit of the step current. The arrays ***Ro*** and ***Rs*** are derived from (21) and (23). The array ***RL*** is analogous to ***Rs***. The arrays ***Rn***, ***Rf***, ***Gn*** and ***Gf*** are created to avoid unnecessary repetition of the computations in the main program.

The half-wave frequencies *fh1* and *fh2* are defined by (12) and (13). The transit times *T1* and *T2* are as defined by (40) and (41). The equations for *dt* and *n2* are defined by (42) and (43).

For transient testing, the signal generator is set to provide square waves at a defined frequency *f*. So the voltage source in the simulation needs to replicate this action. With a square wave, the mark-space ratio is unity and the time *Tmark* the voltage is positive is equal to half the period of the waveform.

Hence

$$Tmark = \frac{1}{2 \cdot f} \tag{50}$$

Since the simulation of time is restricted to a multiple of *dt*, the number of time steps *M* during the period *Tmark* is

$$M = \text{floor}\left(\frac{Tmark}{\text{d}t}\right) \tag{51}$$

where the function floor(*x*) is the greatest integer less than or equal to *x*.

It is also necessary for the simulation to replicate the time *Tscope* it takes for the oscilloscope trace to scan from one side of the graticule to another. The number *N* of time steps involved is

$$N = \text{floor}\left(\frac{Tscope}{dt}\right) \tag{52}$$

The final line at the bottom of Fig. 3 defines the number of time steps in the simulation and the time vector ***t***.

The second page of the worksheet, illustrated in Fig. 4, is a definition of the functions used in the main program.

The function near (*Int1*, *Int2*, ***Vs***) takes the two values of the incident current at the near end and the values of the input voltages, and uses (33) and (25) to calculate values for the reflected current. The output is the values for the reflected currents *Inr1* and *Inr2* and the vector ***Ina*** which records the amplitudes of the currents *Ina1* and *Ina2* at the near end of the line. The function far(*Ifi1*, *Ifi2*) does much the same thing for the parameters at the far end.

The function rad(*Inr*, *Qns*, *Ro*, *Crad*) takes as input the value of the reflected current emanating from the near end, (*Inr1* or *Inr2*) and calculates the amplitude of the current *Int* which actually arrives at the far end, as well as the total charge *Qns* which has departed into the environment. Darney [8] provides a full explanation of the underlying reasoning.

The single-column vector ***F*** provided as input to the function forward(***F***, *Int*, *n*) holds the value of the current *Int* at each section of the *n* segments of the line at a particular instant. The value of this current is placed in the first segment, the contents of every segment are moved forward, and the content of the final segment is provided as output. The action is similar to that of a shift register. The function back(***B***, *Ifr*, *n*) moves data from the far end back to the near end.

The function sqwv(*n, M*) creates a square wave which switches from a value of zero to –*Vg*/2 at the time $t = 0 + dt$, to *Vg*/2 at $t = Tmark$ and back to –*Vg*/2 at $t = 2 \cdot Tmark$. It continues to create a square wave at the frequency *f*.

The function *I*to*V*(*Iprim*, *Iprev*), shown at the top of Fig. 5, takes the value of the current *Iprim* and calculates the value of the voltage *Vout* which would appear at channel 1 input of the oscilloscope. The calculations are based on (46)–(49).

The main program first defines the vectors which simulate the propagation of charges forward and backward along the line. The iterations are carried out for a period of a single scan of the oscilloscope *Tscope*, plus a time equal to *Tmark.* The time *Tmark* coincides with the hold-off period of the oscilloscope before the scan is triggered.

The first two program statements in the iterative section simulate the action of the signal generator. The statements which follow use the output of each function as the input of the next function. Each iteration calculates the values of all the parameters of Fig. 1*c* at time $\boldsymbol{t}_i$. The parameter *j* is set to unity at the end of the simulated hold-off period and starts counting thereafter.

The output vector ***Vsig*** simulates the voltage which would be created by a current transformer clamped round the send conductor,

This is an open access article published by the IET under the Creative Commons Attribution License (http://creativecommons.org/licenses/by/3.0/)

$Lc1 := 3.0 \cdot 10^{-6}$ $Lc2 := Lc1$ $Lc3 := 6.7 \cdot 10^{-6}$

$Cc1 := 1730 \cdot 10^{-12}$ $Cc2 := Cc1$ $Cc3 := 300 \cdot 10^{-12}$

$Rs1 := 8.4$ $Rs2 := 0.2$ $Rs3 := 0.01$

$RL1 := 0$ $RL2 := 0$ $RL3 := 0$

$Crad1 := 300 \cdot 10^{-12}$ $Crad2 := 300 \cdot 10^{-12}$ $Turns := 10$

$RT := 22.7$ $LT := 200 \cdot 10^{-6}$

$K := \frac{50}{50 + 41} = 0.549$ Vch1/Vin

$Vg := 1.62$ peak to peak amplitude of voltage applied to input terminals

$fh1 := 6.93 \cdot 10^{6}$ $T1 := \frac{1}{fh1 \cdot 2} = 7.215 \times 10^{-8}$

$fh2 := 10.26 \cdot 10^{6}$ $T2 := \frac{1}{fh2 \cdot 2} = 4.873 \times 10^{-8}$

$Ro1 := \sqrt{\frac{Lc1}{Cc1}} = 41.643$ $Ro2 := Ro1$

$Ro3 := \sqrt{\frac{Lc3}{Cc3}} = 149.443$

$$\boldsymbol{Ro} := \begin{pmatrix} Ro1 + Ro2 & -Ro2 \\ -Ro2 & Ro2 + Ro3 \end{pmatrix}$$

$$\boldsymbol{Rs} := \begin{pmatrix} Rs1 + Rs2 & -Rs2 \\ -Rs2 & Rs2 + Rs3 \end{pmatrix}$$

$$\boldsymbol{RL} := \begin{pmatrix} RL1 + RL2 & -RL2 \\ -RL2 & RL2 + RL3 \end{pmatrix}$$

$\boldsymbol{Rn} := \boldsymbol{Ro} + \boldsymbol{Rs}$ $\boldsymbol{Gn} := \boldsymbol{Rn}^{-1}$

$\boldsymbol{Rf} := \boldsymbol{Ro} + \boldsymbol{RL}$ $\boldsymbol{Gf} := \boldsymbol{Rf}^{-1}$

$n1 := 15$ $dt := \frac{T1}{n1} = 4.81 \times 10^{-9}$ $n2 := ceil\left(n1 \cdot \frac{T2}{T1}\right) = 11$

$f := 200 \cdot 10^{3}$

$Tmark := \frac{1}{2 \cdot f} = 2.5 \times 10^{-6}$ $M := floor\left(\frac{Tmark}{dt}\right)$

$Tscope := 5 \cdot 10^{-6}$ $N := floor\left(\frac{Tscope}{dt}\right)$

$n := 1 .. N$ $\boldsymbol{t}_n := n \cdot dt$

Fig. 3 *Copy of the first page of the worksheet. Definition of input parameters*

Vret is proportional to the current in the return conductor, and ***Vgnd*** is proportional to the current in the structure. ***Vch1*** is a record of the voltage which would be monitored by channel 1 of the oscilloscope. This worksheet can be downloaded [9].

3.7. Test results

A series of tests were carried out on the rig of Fig. 1*a* with the signal generator set to give a square wave output. As with the frequency response tests, channel 1 of the oscilloscope was used to monitor the input voltage at the terminals at the near end of the line, and channel 2 was used to monitor the output of the current transformer. This was done at a number of frequencies *f* of the square wave, and the waveform observed on the screen was compared with that of the simulation.

Initially, there were significant deviations between theoretical and test results. However, when the model was modified to include the effect of the inductance of the current transformer and the effect of radiated emission, a close correlation was achieved.

Fig. 6 illustrates the results of just one of the tests carried out. The current transformer was clamped round both conductors (send and return), to measure the common-mode current. Then the signal generator was set to give a square waveform at 200 kHz, the amplitude of the voltage step varied to set the value of *Vch1* to 0.8 V, and the time period on the oscilloscope selected to give the waveform of a

This is an open access article published by the IET under the Creative Commons Attribution License (http://creativecommons.org/licenses/by/3.0/)

doi: 10.1049/joe.2017.0382

$$near(Ini1, Ini2, Vs) := \left| \begin{array}{l} Ini \leftarrow \begin{pmatrix} Ini1 \\ Ini2 \end{pmatrix} \\ Ina \leftarrow Gn \cdot (2 \cdot Ro \cdot Ini + Vs) \\ Inr \leftarrow Ina - Ini \\ \begin{pmatrix} Inr_1 & Inr_2 & Ina \end{pmatrix} \end{array} \right.$$

$$far(Ifi1, Ifi2) := \left| \begin{array}{l} Ifi \leftarrow \begin{pmatrix} Ifi1 \\ Ifi2 \end{pmatrix} \\ Ifa \leftarrow Gf \cdot (2 \cdot Ro \cdot Ifi) \\ Ifr \leftarrow Ifa - Ifi \\ \begin{pmatrix} Ifr_1 & Ifr_2 & Ifa \end{pmatrix} \end{array} \right.$$

$$rad(Inr, Qns, Ro, Crad) := \left| \begin{array}{l} Int \leftarrow \dfrac{Qns}{Ro \cdot Crad} \\ Ins \leftarrow Inr - Int \\ Qns \leftarrow Qns + Ins \cdot dt \\ (Int \quad Qns) \end{array} \right.$$

$$forward(F, Inr, n) := \left| \begin{array}{l} F_1 \leftarrow Inr \\ for \ \ i \in n + 1 \ldots 1 \\ \quad F_{i+1} \leftarrow F_i \\ Ifi \leftarrow F_{n+2} \\ (F \quad Ifi) \end{array} \right.$$

$$back(B, Ifr, n) := \left| \begin{array}{l} B_{n+1} \leftarrow Ifr \\ for \ \ i \in 2 \ldots n + 1 \\ \quad B_{i-1} \leftarrow B_i \\ Ini \leftarrow B_1 \\ (B \quad Ini) \end{array} \right.$$

$$sqwv(n, M) := \left| \begin{array}{l} x \leftarrow trunc\left(\dfrac{n-2}{M}\right) \\ sgn \leftarrow \left| \begin{array}{ll} -1 & if \ \ 2 \cdot floor\left(\dfrac{x}{2}\right) = x \\ 0 & if \ \ n < 2 \\ 1 & otherwise \end{array} \right. \\ \dfrac{Vg}{2} \cdot sgn \end{array} \right.$$

Fig. 4 *Copy of the second page of the worksheet. Definition of the functions*

single cycle. Fig. 6*a* is a copy of the photograph taken of that display. Fig. 6*c* is a photo of the waveform on channel 2.

The input parameters on the first page of the worksheet were adjusted to set the voltage *Vg* to 1.62 V and the frequency of the simulation to 200 kHz, and a record taken of the graphs of the vectors ***Vch1*** and ***Vch2***. These are displayed in Figs. 6*b* and *d*. ***Vch2*** is a copy of the vector ***Vgnd*** in Fig. 5.

The close correlation between the test and simulated waveforms provides a high degree of confidence in the modelling technique. Of particular interest is the sawtooth appearance of the waveforms of Figs. 6*c* and *d*. This is because the step change in the common-mode current arrives back at the near end before that of the differential-mode current.

3.8. *Steady-state conditions*

The main program illustrated in Fig. 5 was altered to compute the response of the model to a step pulse of 5 µs duration. Currents in all three conductors are simulated.

The red curve at the top of the graph of Fig. 7*a* simulates the waveform of the current ***Isig*** in the send conductor. This is the differential-mode current. The dashed green curve at bottom of the graph simulates the current ***Ignd*** in conductor 3, the 15 mm copper tube. This curve correlates with ***Vch2*** of Fig. 6*d*. ***Ignd*** is the common-mode current. The blue curve simulates the current ***Iret*** in the return conductor. It can be seen that most of the return current flows in the return conductor. That is, during the first 5 µs, the differential-mode loop carries most of the electromagnetic energy.

When the time frame of the simulation is increased to 50 µs, as shown in Fig. 7*b*, things begin to change. Current in the copper tube continues to rise, and after 250 µs, current in the common-mode loop exceeds that in the differential-mode loop.

Fig. 7*c* shows that the current in the copper tube continues its inexorable rise, and at 500 µs, almost all of the return current flows in the tube. Current in the return conductor becomes insignificant. At 5 ms the currents are

$$\begin{aligned} Ic1 &= 0.193 \text{ A} \\ Ic2 &= 9.173 \times 10^{-3} \text{ A} \\ Ic3 &= 0.183 \text{ A} \end{aligned} \tag{53}$$

These are precisely the values of the currents which would flow on the conductors of the model of Fig. 1*b* were the voltage source *Vg* to be a 1.62 V battery. However, this apparent 'steady-state' condition only arises after more than a million traverses have been made of the leading edge of the step pulse, and it is sustained by imperceptible oscillations at about 10 MHz. This worksheet is available at [9].

4. Assessment

4.1. *Photons and charges*

It has been shown that the transient behaviour of the electromagnetic coupling between the three conductors can be visualised and analysed as a system of moving charges which propagate forwards and backwards along the conductors. What is not immediately obvious is that charges propagate to and fro between the conductors. During the first 5 ns after the appearance of the step voltage, charges flow from the send conductor, across the gap into the other two conductors, back along those conductors, and then back across the gap into the send conductor. This deduction supports that made during the transient analysis of an open-circuit cable [10].

In fact, this assumption is inherent in the basic transmission line equations

$$\begin{aligned} (R + j \cdot \omega \cdot L) \cdot dx \cdot I &= V - \left(V + \frac{\delta V}{\delta x} \cdot dx\right) = -\frac{\delta V}{\delta x} \cdot dx \\ (G + j \cdot \omega \cdot C) \cdot dx \cdot V &= I - \left(I + \frac{\delta I}{\delta x} \cdot dx\right) = -\frac{\delta I}{\delta x} \cdot dx \end{aligned} \tag{54}$$

The very existence of this pair of equations depends on the assumption that current flows from the return conductor back into the send conductor. Figure C.1 of [11] illustrates this. Current is due to the flow of charges. Voltage changes when charges move.

This is an open access article published by the IET under the Creative Commons Attribution License (http://creativecommons.org/licenses/by/3.0/)

$$
\begin{aligned}
&ItoV(Iprim, Iprev) := \left|
\begin{array}{l}
Isec \leftarrow \dfrac{Iprim}{Turns} \\
dI \leftarrow \dfrac{dt}{LT} \cdot RT \cdot (Isec - Iprev) \\
Iprev \leftarrow Iprev + dI \\
Vout \leftarrow RT \cdot (Isec - Iprev) \\
(Vout \quad Iprev)
\end{array}
\right. \\
&(\mathbf{Vch1} \quad \mathbf{Vsig} \quad \mathbf{Vret} \quad \mathbf{Vch2}) := \left|
\begin{array}{l}
\mathbf{F1}_{n1+2} \leftarrow 0 \\
\mathbf{F2}_{n2+2} \leftarrow 0 \\
\mathbf{B1}_{n1+1} \leftarrow 0 \\
\mathbf{B2}_{n2+1} \leftarrow 0 \\
for \quad i \in 1 .. M + N \\
\quad \left|
\begin{array}{l}
\mathbf{Vgen}_1 \leftarrow sqwv(i, M) \\
\mathbf{Vgen}_2 \leftarrow 0 \\
(Inr1 \quad Inr2 \quad \mathbf{Ina}) \leftarrow near(Ini1, Ini2, \mathbf{Vgen}) \\
(Int1 \quad Qns1) \leftarrow rad(Inr1, Qns1, Ro1, Crad1) \\
(Int2 \quad Qns2) \leftarrow rad(Inr2, Qns2, Ro2, Crad2) \\
(\mathbf{F1} \quad Ifi1) \leftarrow forward(\mathbf{F1}, Int1, n1) \\
(\mathbf{F2} \quad Ifi2) \leftarrow forward(\mathbf{F2}, Int2, n2) \\
(Ifr1 \quad Ifr2 \quad \mathbf{Ifa}) \leftarrow far(Ifi1, Ifi2) \\
(\mathbf{B1} \quad Ini1) \leftarrow back(\mathbf{B1}, Ifr1, n1) \\
(\mathbf{B2} \quad Ini2) \leftarrow back(\mathbf{B2}, Ifr2, n2) \\
(Vout1 \quad Iprev1) \leftarrow ItoV(\mathbf{Ina}_1, Iprev1) \\
(Vout2 \quad Iprev2) \leftarrow ItoV(\mathbf{Ina}_2, Iprev2) \\
j \leftarrow 1 \\
j \leftarrow i - M \quad if \quad i > M \\
\mathbf{Vsig}_j \leftarrow Vout1 \\
\mathbf{Vgnd}_j \leftarrow Vout2 \\
\mathbf{Vret}_j \leftarrow Vout1 - Vout2 \\
\mathbf{Vch1}_j \leftarrow K \cdot (\mathbf{Vgen}_1 - Rs1 \cdot \mathbf{Ina}_1)
\end{array}
\right. \\
(\mathbf{Vch1} \quad \mathbf{Vsig} \quad \mathbf{Vret} \quad \mathbf{Vgnd})
\end{array}
\right.
\end{aligned}
$$

Fig. 5 *Copy of the third page of the worksheet. The main program*

The problem with this visualisation is that the charges do not flow through the insulation material. The entity involved in the propagation of electromagnetic energy is the photon, and photons do not carry charge [12]. However, if it is assumed that when a photon departs from an atom, it leaves a charge on that atom and that when it arrives at another atom it creates a charge on that second atom, then a possible explanation emerges. It is photons which actually carry the electromagnetic energy, and the interaction of photons with atoms creates a system of moving charges which can be analysed using the concepts of circuit design.

In this particular example, it can be reasoned that most of the return current flows in the return conductor during the first 5 μs because its surface is closest to the send conductor. After 5 ms, most of the return current flows via the structure, because its surface area is so much greater.

4.2. *Equipotential ground*

This concept is illustrated in books on electromagnetic theory as a line at the bottom of a circuit diagram which does not possess the properties of inductance, capacitance or resistance. '*Figure 12-3 Lumped constant representation of a transmission line*' in [13] is one example. In [14], it is shown how this representation simplifies the analysis by subsuming the properties of the return conductor into those of the send conductor. The problem with this simplification is that it assumes that the interaction between the return

This is an open access article published by the IET under the Creative Commons Attribution License (http://creativecommons.org/licenses/by/3.0/)

doi: 10.1049/joe.2017.0382

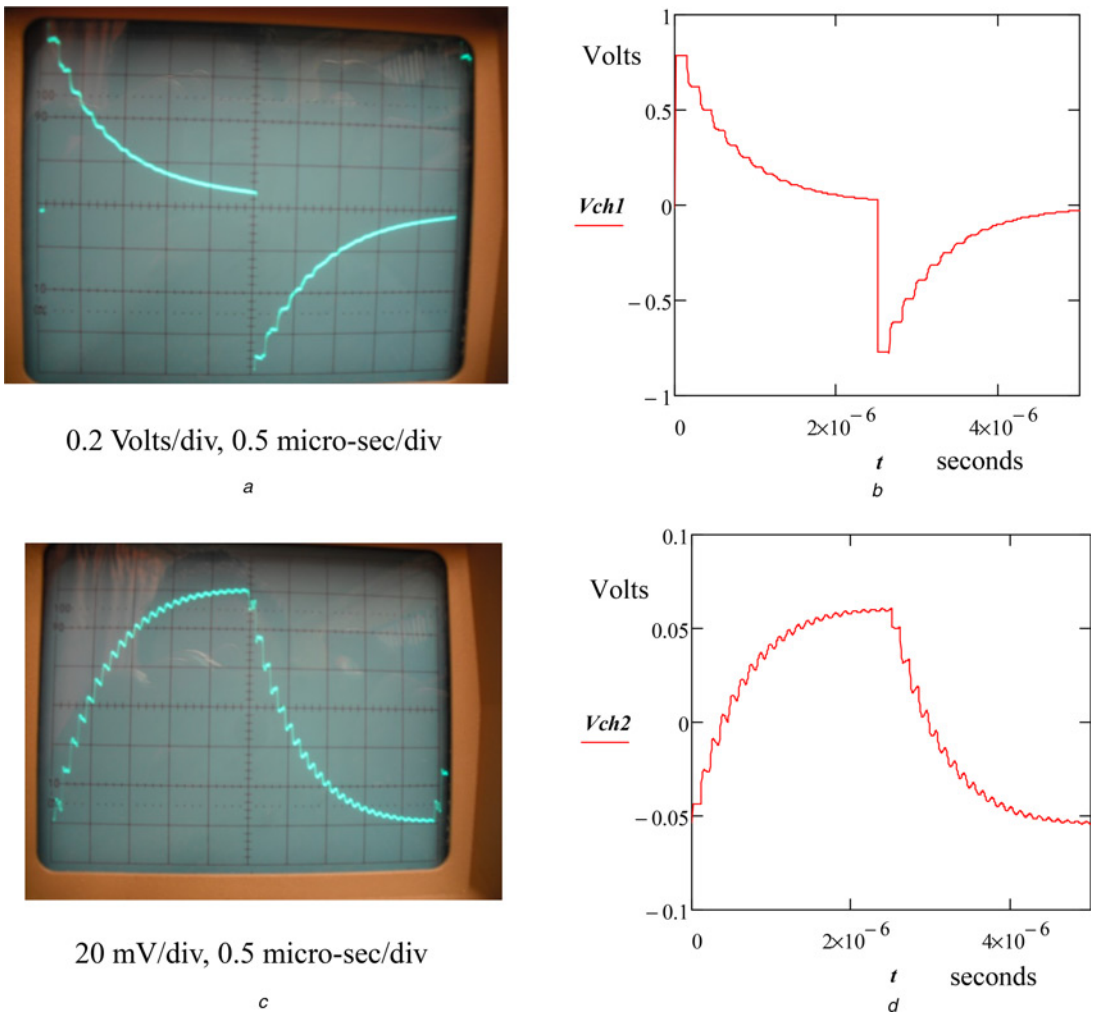

Fig. 6 *Compared the test results with the simulation*
a Waveform of the input voltage, as monitored by channel 1 of the oscilloscope
b Simulated waveform at channel 1, ***Vch1***
c Waveform of the current in the common-mode loop, as displayed by channel 2
d Simulated waveform at channel 2, ***Vch2***

conductor and the ground is not relevant. Invoking the concept renders impossible any analysis of the coupling between the three conductors of the signal link. It eliminates any chance of analysing EMI.

This analysis has shown that when the structure is used to carry any return current, it creates a situation where a vast number of charges are propagating backwards and forwards along that structure. This manifests itself as a high magnetic field which permeates the whole system. If the current in the send conductor switches off, the unwanted dynamic energy possessed by the current in the structure will spread far and wide and reappear as interference in other parts of the system.

The fact that the resistance of the structure of vehicles is extremely low leads many engineers to utilise it as a general-purpose return conductor for power supplies, actuators, and sensors. It is reasoned that the inclusion of dedicated return conductors would result in a needless increase in the weight and cost of the system under review. Such a design decision is the cause of innumerable EMI problems. It results in unexpected failures during formal EMC testing.

It is possible that the disastrous loss of Flight 800 [15] was due to the transient current in the structure coupling energy into the wiring of the fuel level sensors in the centre tank. Any bad joint in the wiring could have caused a high voltage to develop across the gap and the resulting spark could have ignited the fuel. It may or may not be the case that such a mechanism was the actual cause of the disaster, but it is definitely a hazard condition which needs to be analysed during the design of aircraft.

4.3. Single-point ground.

A succinct definition [16] of this concept is:

> 'A single-point ground system is one in which subsystem ground returns are tied to a single point within that subsystem. The intent of using a single-point ground system is to prevent currents of two different subsystems from sharing the same return path and producing common impedance coupling.' The fallacy in this reasoning is the fact that it ignores the existence of the send conductors.

It is the send conductor which is the source of electromagnetic energy. First and foremost, this conductor acts as a transmitting antenna. The energy it transmits goes where it can. This energy can be visualised as the dynamic energy of moving charges. In conductors, this manifests itself as current flow. The return current follows whatever path it can find. It does not necessarily follow the path designated by the system designer.

This is an open access article published by the IET under the Creative Commons Attribution License (http://creativecommons.org/licenses/by/3.0/)

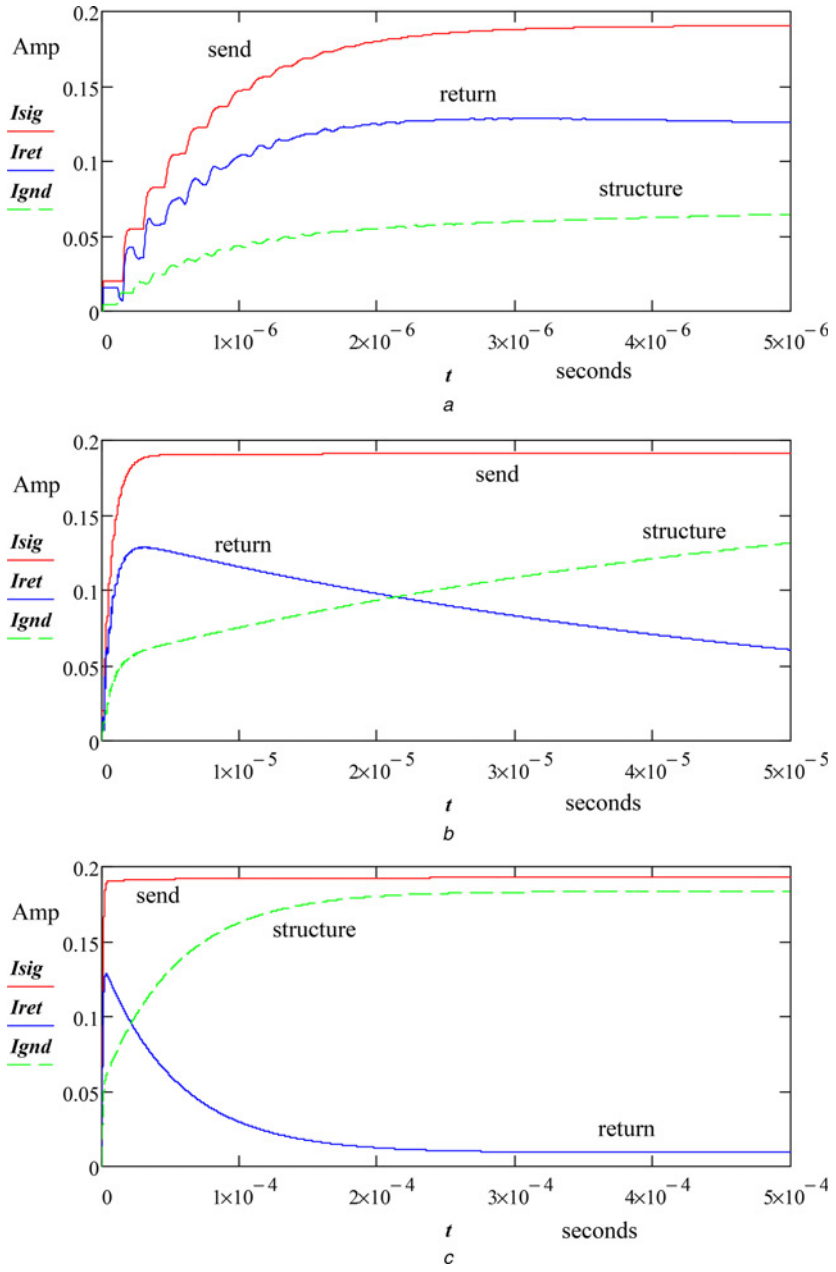

Fig. 7 *Response of current in each conductor to a step voltage input*
a After 5 μs
b After 50 μs
c After 500 μs

If a designated conductor is provided to carry return current and is located as close as possible to the send conductor, then the electromagnetic energy automatically follows the path defined by the routing of the cable. If the return conductor is deliberately separated from the send conductor, electromagnetic energy spreads far and wide.

The action of implementing a single-point ground in any system guarantees that such a system will experience EMI problems during its entire existence.

5. Conclusion

The above analysis has shown that it is possible to create models which simulate the cross-coupling between the differential-mode and the common-mode currents in a test rig, in both the frequency domain and the time domain, using the analytical tools of Circuit Theory. The frequency simulation has proved to be accurate over the entire range covered by Electromagnetic Theory. The analysis in the time domain has been demonstrated to be accurate from 10 ns to steady-state conditions. This process can be used to analyse the coupling between cable and conducting structure in any electrical system. EMI can be analysed without recourse to the complexities of full-field modelling.

It is a dangerous practice to treat the conducting structure as a general-purpose return conductor; its surface is certainly not equipotential. The fallacy in the 'single-point ground' concept has been identified.

6 References

[1] Darney I.B.: 'Lumped parameter models', in Duffy A. (Ed.): 'Circuit modeling for electromagnetic compatibility' (SciTech Publishing, Edison, NJ, 2013), pp. 47–48

This is an open access article published by the IET under the Creative Commons Attribution License (http://creativecommons.org/licenses/by/3.0/)

[2] Darney I.B.: 'Bench testing', in Duffy A. (Ed.): 'Circuit modeling for electromagnetic compatibility' (SciTech Publishing, Edison, NJ, 2013), pp. 183–188
[3] Darney I.B.: 'Transmission line models', in Duffy A. (Ed.): 'Circuit modeling for electromagnetic compatibility' (SciTech Publishing, Edison, NJ, 2013), p. 86
[4] Darney I.B.: 'Bench testing', in Duffy A. (Ed.): 'Circuit modeling for electromagnetic compatibility' (SciTech Publishing, Edison, NJ, 2013), pp. 197–206
[5] http://www.designemc.info/CrossCoupFreq.zip, accessed on September 5 2017
[6] Skitek G.G., Marshall S.V.: 'Transmission lines' in 'Electromagnetic concepts and applications' (Prentice-Hall Inc., Englewood Cliffs, NJ, 1982), p. 411
[7] Skitek G.G., Marshall S.V.: 'Transmission lines' in 'Electromagnetic concepts and applications' (Prentice-Hall Inc., Englewood Cliffs, NJ, 1982), p. 381
[8] Darney I.B.: 'Transient analysis', in Duffy A. (Ed.): 'Circuit modeling for electromagnetic compatibility' (SciTech Publishing, Edison, NJ, 2013), pp. 155–161
[9] http://www.designemc.info/CrossCoupTran.zip, accessed on September 5 2017
[10] Darney I.B.: 'Modelling the transient emission from a twin conductor cable', IET J. Eng., 2015, p. 1. https://doi.org/10.1049/joe.2015.0193
[11] Darney I.B.: 'Appendix C. The hybrid equations', in Duffy A. (Ed.): 'Circuit modeling for electromagnetic compatibility' (SciTech Publishing, Edison, NJ, 2013), p. 274
[12] https://en.wikipedia.org/wiki/Photon, accessed on September 6 2017
[13] Skitek G.G., Marshall S.V.: 'Transmission lines', in Duffy A. (Ed.): 'Electromagnetic concepts and applications' (Prentice- Hall, Inc., Englewood Cliffs, NJ, 1982), p. 373
[14] Plonus M.A.: 'Transmission lines', in 'Applied electromagnetics', (McGraw-Hill Book Company, NY, 1978), p. 554
[15] https://www.ntsb.gov/investigations/AccidentReports/Reports/AAR0003.pdf, accessed on September 5 2017
[16] Paul C.R.: 'System design for EMC', in Chang K. (Ed.): 'Introduction to electromagnetic compatibility' (John Wiley & Son, NY, 1992, 1st edn.), p. 700

This is an open access article published by the IET under the Creative Commons Attribution License (http://creativecommons.org/licenses/by/3.0/)